

Induced exchange and spin-orbit effects by proximity in graphene on Ni and Co

Mayra Peralta,^{1,2,*} Ernesto Medina,^{2,3} and Francisco Mireles^{1,†}

¹*Departamento de Física - Centro de Nanociencias y Nanotecnología,*

Universidad Nacional Autónoma de México, Apdo. Postal 14, 22800 Ensenada, Baja California, México

²*Yachay Tech University, School of Physical Sciences & Nanotechnology, 100119-Urcuquí, Ecuador*

³*Centro de Física, Instituto Venezolano de Investigaciones Científicas, 21827, Caracas 1020 A, Venezuela.*

(Dated: March 19, 2019)

The induced-proximity effects of nearly commensurate lattice structure of a graphene layer on Ni(111) and Co(0001) substrates in the AC stacking configuration are addressed through an analytical tight-binding approach within the Slater-Koster method. A minimal Hamiltonian is constructed by considering the hybridizations of the magnetic 3d-orbitals of Ni(Co) atoms with the p_z -orbitals of graphene, in addition to the atomic spin-orbit coupling and the magnetization of the Ni(Co) atoms. A low-energy effective Hamiltonian for graphene/Ni(Co) describing the perturbed π -bands in the vicinity of the Dirac points is derived which enable us to get further insight on the physical nature of the induced-effective couplings to the graphene layer. It is shown that a magneto-spin-orbit type effect may emerge through two competing mechanisms simultaneously present, namely the proximity induced exchange and Rashba spin-orbit interaction. Such effects results in giant exchange splittings and robust Rashba spin-orbit coupling transferred to the graphene layer in agreement with recent density functional theory calculations and experimental observations. We further analyze the physical conditions for the appearance of intact Dirac cones in the minority spin bands as observed by recent photoemission measurements with spin resolution.

I. INTRODUCTION

Graphene in proximity with metallic substrates may acquire fascinating new electronic and magnetic properties.^{1,2} Depending upon the appropriate substrate, a number of interesting features may arise in its band structure, such as the appearance of an energy gap between the π (electron) and π^* (hole) bands, the shifting of the Fermi energy E_F of the Dirac cone, distortions of its linear dispersion, and the formation of local band gaps.³⁻⁷ The main known mechanisms responsible for these band modifications are in one hand, the strong hybridization between the $2p_z$ orbitals of the carbon atoms with the d -states of the metallic layer, and on the other, the sublattice symmetry breaking. Remarkably, these proximity effects may also promote the emergence of the anomalous Hall effect in graphene/ferromagnetic films,⁸ quantum spin-Hall phases in graphene/topological-insulating interfaces,⁹ and the enhancement of the Rashba spin-orbit interaction.¹⁰⁻¹⁶

The topic of induced spin-orbit effects in graphene by proximity is of especial prominence for spintronics applications given the smallness of intrinsic spin-orbit splitting effects in freestanding graphene ($\lesssim 50 \mu\text{eV}$).^{17,18} There is a strong experimental evidence that the epitaxial synthesis of graphene interfaces with high spin-orbit metals (*e.g.* Au, Ag, Pb) intercalated or in direct contact with different substrates such as Ir, Ni, and Co, leads to unusually large Rashba spin-orbit splittings of the Dirac cones that ranges between 13-100 meVs.^{10-14,19} It is also established that the proximity spin-orbit coupling increases with the atomic number of the transition metal. As supported by several density functional theory (DFT) studies,^{4,10,13,19} the rather anomalous increase of the spin-splitting is as-

cribed to a strong π - d hybridization between graphene and the substrate and/or the intercalated layer.

The direct proximity with ferromagnetic substrates, on the other hand, leads to a natural breaking of time reversal symmetry and to the transfer of exchange fields to graphene.²⁰⁻²³ This exchange coupling in conjunction with spin-orbit interaction opens the possibility of a wider spin-dependent extension of graphene outstanding characteristics.²⁴ It is important to remark that in the process of transferring ferromagnetic properties to graphene, it is also highly desirable to preserve its attractive features of robust mobility and linearity of its electronic bands near the Fermi level.^{10,25} These physical conditions have proved however, to be extremely challenging to realize experimentally. For instance, recent experiments^{10,21,25} have reported that the synthesis of graphene on ferromagnetic Ni(111) and Co(0001) in the AC stacking configuration, leads to strong exchange splittings with the preservation of the linearity of the bands at the Dirac point, however no Rashba coupling splitting was observed in these experiments.

More recent angle- and spin-resolved photoemission experiments (SARPES) by Rybkin et al.²⁶ investigated the spin-dependent band splitting in graphene/Co(0001) intercalated with Au. Their measurements suggests that the combined action of a strong exchange and Rashba coupling in quasi-freestanding graphene is indeed possible. From the analysis of their spin-resolved photoemission spectra and DFT calculations the authors were able to determine the existence of a strong Rashba spin-orbit splitting of around 57 meV (most likely due to the Au atoms) and a giant exchange splitting of the Dirac cone of ~ 175 meV; all this whiles the linear dispersion was nevertheless largely preserved comprising evidence of a so called magneto-spin-orbit effect.²⁶ However, the presence

of Co atoms into the intercalated Au layer was not fully excluded in their XPS analysis. Clearly there is a need of a deeper understanding at the microscopical level of the physical nature of the proximity induced Rashba and exchange couplings, its magnitude estimates, as well as its interplay in graphene/ferromagnetic interfaces. Having a better understanding of these coupling mechanisms could also serve as an excellent platform to investigate, interesting topological phenomena and the realization of the quantum anomalous Hall effect, in addition to its relevance for applied studies in new spintronic devices.

Motivated by these works, the aim of this paper is to introduce a simplified microscopic theoretical model of the effective interactions in a AC stacking graphene/Ni and graphene/Co interfaces based in a nearest-neighbor multiorbital tight-binding approach. The model will allow us to gain further insight to the origins of the observed large Rashba spin-orbit and exchange couplings, proximity-induced at the graphene layer, and its relative estimates. Although our primary interest here is on Ni and Co substrates, our results are applicable to a broad range of $3d$ -ferromagnetic metals, as we expect that the overall qualitative features of the proximity induced exchange and spin-orbit coupling effects shall hold as well. The study permits to explore on the microscopic physical conditions that leads to the observed preservation of the linearity of the bands despite the strong π - d hybridization in such interfaces. In particular, we derive an effective low energy Hamiltonian for graphene/Ni and graphene/Co in the vicinity of the $K(K')$ Dirac points that captures the main characteristics of the bands reported experimentally and by DFT studies for the case of graphene/Ni and graphene/Co^{10,25,27} yielding as well a qualitative resemblance to the observed results of a magneto-spin-orbit effect in graphene/Au/Co interfaces.^{26,28} The model helps us to determine which $3d$ -orbitals of the ferromagnetic layer participate predominantly in the strong hybridizations with the π -bands and originates the linear electronic structure in the vicinity of the Dirac point. We also analyze the appearance of intact (unperturbed) Dirac cones in the minority spin bands observed by several angle- and spin-resolved photoemission experiments.^{25,27,28}

II. MODEL

A. Graphene/Ni(Co) Interface

Consider a graphene monolayer deposited on a magnetized nickel(cobalt) substrate in which the arrangements of magnetic atoms form a commensurate lattice with negligible mismatch. The layered system is supposed to be strainless and without disorder. In order to study the interactions between graphene and a Ni(Co) substrate we will consider only the Ni(Co) upper layer in contact with graphene, as the magnetic couplings are expected to decay exponentially with the distance. It has been reported that the the most stable vertical arrangement

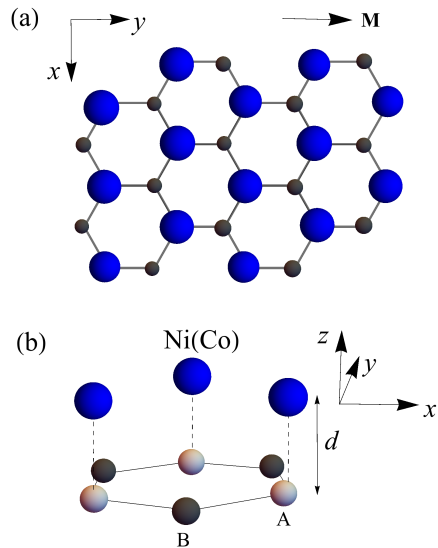


FIG. 1. Schematic of the graphene/Ni(Co) under study. (a): Top view of the configuration studied (AC stacking), where Ni(Co) atoms are directly over the atoms of sublattice A and atoms of the sublattice B are in the hcp sites of the Ni(Co) lattice. The direction of the Ni(Co) magnetic moment $\mathbf{M} = M\hat{y}$ is shown. (b): 3D view of a single graphene hexagon which shows the Ni(Co)-graphene distance d .

of the atoms^{21,27} is the AC stacking configuration for both substrates, in which the Ni(Co) atoms are placed directly over the atoms of sublattice A of graphene and atoms of the sublattice B are in the hcp sites of the Ni(Co) lattice, Fig. 1(a). The equilibrium Ni-graphene distance reported in the literature¹³ for this configuration is of $d = 2.05\text{\AA}$, while the similar distance between Co-graphene is reported²⁷ to be 2.11\AA (see Fig. 1(b)). In addition we will assume that the magnetic coupling between nickel(cobalt) atoms is negligible. Henceforth, as indicated in Fig. 1(a), the direction of the magnetization (magnetic moment), \mathbf{M} , for the Ni(Co) layer is chosen along the y -axis.

B. Tight-binding model and Low Energy Effective Hamiltonian

The simplest nearest-neighbor tight-binding model that describes graphene in contact with a ferromagnet metal interface in the AC-stacking configuration shall takes into account the carbon valence $2p_z$ orbitals that form the electron π and hole π^* bands in pristine graphene, and the outer shell orbitals of nickel(cobalt) atoms, namely $3d_{xy}$, $3d_{xz}$, $3d_{yz}$, $3d_{3z^2-r^2}$, and $3d_{x^2-y^2}$ orbitals.^{17,18} We consider a two center tight-binding Hamiltonian that incorporates the atomic spin-orbit interaction and the exchange field due the nearby nickel(cobalt) atoms. A Slater-Koster Hamiltonian that dictates the main hybridization properties is constructed with matrix elements of the form $\langle \phi_{\mu,s} | \hat{H}_{TB} | \phi_{\mu',s'} \rangle$ where

$\mu = \{0, 1, 2, 3, 4, 5, 6\}$ denotes the $2p_z^{A/B}$ orbitals of carbon atoms and the five $3d$ -orbitals of nickel(cobalt), and $s = \{\uparrow, \downarrow\}$ labels the electron spin, yielding a 14×14 overlapping matrix for the graphene/Ni(Co) interface (Appendix A). A low energy 4×4 effective Hamiltonian in the momentum space is then derived and it has the compact form at the $K(K')$ valley

$$\mathcal{H}_{\text{eff}}(\mathbf{p}) = (\boldsymbol{\sigma} \cdot \mathbf{p}) \otimes (v_F^* s_o - v_d^* s_y) + \lambda_{XR} (\boldsymbol{\sigma} \otimes \mathbf{s})_z + \mathcal{E}_{ex}, \quad (1)$$

where $\boldsymbol{\sigma} = (\xi \sigma_x, \sigma_y)$ is the Pauli vector matrix acting on the sublattice $\{A, B\}$ in pristine graphene, with $\xi = +1(-1)$ for the $K(K')$ valley, respectively, \mathbf{p} is the momentum operator, $\mathbf{s} = (s_x, s_y, s_z)$ is the Pauli vector matrix that acts on the real spin, with s_o the unit matrix in spin-space. In Eq. (1) the first term to the right corresponds to an effective Dirac term linear in momentum with a velocity v_F^* diagonal in spin-space shifted by an off-diagonal exchange field dependent velocity term v_d^* . The second term has the form of a Rashba spin-orbit interaction $(\boldsymbol{\sigma} \otimes \mathbf{s})_z \equiv \xi \sigma_x \otimes s_y - \sigma_y \otimes s_x$, with a coupling parameter λ_{XR} . The proximity-induced Rashba term is present due the hybridization of the p_z -orbitals with the $d_{3z^2-r^2}$ as well as for the presence to the on-site exchange field of nickel(cobalt) atoms. Lastly the term \mathcal{E}_{ex} represent a constant matrix which effectively induces an exchange-dependent energy shifting of the Dirac cones together with a exchange-field transfer to the graphene layer along the magnetization orientation of the ferromagnetic substrate. As we shall discuss, the interplay of the last two terms in Eq. (1) accounts for the magneto-spin-orbit effect. The model effective Hamiltonian described in Eq. (1) captures very well the main features of the observed low energy bands and to first principles calculations of graphene on nickel(cobalt), as discussed in detail in the next sections.

We find that the reduced velocity $v_F^* = v_F + \eta_d \Delta_0$ and $v_d^* = \eta_d \Delta_{ex}$, where $v_F = -\frac{\sqrt{3}a}{2\hbar} V_{pp\pi}$ is the Fermi velocity for freestanding graphene in terms of the relevant Slater-Koster overlapping integral between carbon-carbon atoms, and a is the lattice parameter. The on-site energy of nickel(cobalt) atoms relative to the p -states of carbon is $\Delta_0 = \varepsilon_{d_0} - \varepsilon_p$, while Δ_{ex} represents the exchange energy spin-splitting at the nickel(cobalt) atoms. The parameter η_d depends on the overlapping p_z - d matrix elements and on the exchange field through the expression,

$$\eta_d = \frac{\sqrt{3}a}{2\hbar} \frac{U_{p_z, z^2}^A U_{p_z, z^2}^B}{\Delta_0^2 - \Delta_{ex}^2}, \quad (2)$$

The matrix elements $U_{p_z, z^2}^{A/B}$ are written in terms of the Slater-Koster parameters $U_{pd\sigma}$ and $U_{pd\pi}$ (see Table I for the estimated graphene/Ni parameters).²⁹ The induced exchange-Rashba p_z - d coupling is dictated by the parameter

$$\lambda_{XR} = \frac{3}{2} \frac{\sqrt{3}b \xi_d \Delta_0 \Delta_1}{(\Delta_1^2 - \Delta_{ex}^2)(\Delta_0^2 - \Delta_{ex}^2)} U_{p_z, z^2}^A \tilde{U}_{p_z, xz}^B, \quad (3)$$

where $\Delta_1 = \varepsilon_{d_1} - \varepsilon_p$, where ε_{d_i} , with $i = 0, 1$ are the relevant onsite energies for Co(Ni), see Appendix A. Notice that the breaking of the inversion symmetry by the Rashba term does not come from a Stark-type effect, as no external electric field is considered here, but from the close proximity to the ferromagnetic atoms instead, due to its relatively large spin-orbit coupling. Indeed, it is proportional to the intrinsic spin-orbit parameter of nickel(cobalt) ξ_d , to the effective distance b between the nickel(cobalt) atom to its nearest-neighbour carbon atom, as well as, to the overlap energies between the p_z -orbital of graphene atoms of sublattice B with $d_{xz, yz}$ orbitals of nickel(cobalt) atoms, $\tilde{U}_{p_z, xz}^B$; and the overlap of p_z -orbitals of graphene's atoms of sublattice A and d_{z^2} orbitals of nickel(cobalt) atoms, U_{p_z, z^2}^A . It also has a nontrivial functional dependence in Δ_{ex} . The last term in Eq. (1) has two contributions,

$$\mathcal{E}_{ex} = \varepsilon_{pd} \otimes s_y + \varepsilon_D^* \otimes s_o. \quad (4)$$

the first will contribute to a spin-dependent mass term as well as the opening of an energy gap, explicitly $\varepsilon_{pd} = \Delta_+ s_o + \Delta_- s_z$. The second yields a uniform energy shift of the Dirac cones, $\varepsilon_D^* = \varepsilon_- s_o + \varepsilon_+ s_z$, in which

$$2\Delta_{\pm} = [\varepsilon_1 \pm (\varepsilon_2 + \varepsilon_3)] \Delta_{ex}, \quad (5)$$

$$2\varepsilon_{\pm} = -\varepsilon_1 \Delta_0 \pm (\varepsilon_2 \Delta_1 + \varepsilon_3 \Delta_0), \quad (6)$$

where we have found that the dimensionless parameters ε_i , ($i = 1, 2, 3$) have the explicit form

$$\begin{aligned} \varepsilon_1 &= \frac{(U_{p_z, z^2}^A)^2}{\Delta_0^2 - \Delta_{ex}^2}, \\ \varepsilon_2 &= \frac{3b^2}{4(\Delta_1^2 - \Delta_{ex}^2)} \left[b^2 (\tilde{U}_{p_z, xy}^B)^2 + 4(\tilde{U}_{p_z, xz}^B)^2 \right], \\ \varepsilon_3 &= \frac{3(U_{p_z, z^2}^B)^2}{\Delta_0^2 - \Delta_{ex}^2}, \end{aligned} \quad (7)$$

in which effective Slater-Koster energies $\tilde{U}_{p_z, xy}^B$ and $\tilde{U}_{p_z, xz}^B$ depend on the relative orientation of the atomic orbitals (Appendix A).

C. Low Energy Dispersion for Graphene/Ni

The low energy band structure is obtained by diagonalizing the effective Hamiltonian of Eq. (1) using the tight-binding related parameters contained in Table I and II. Note that for Ni we have $\xi_d \simeq 2\Delta_{ex}$. However, for illustration purposes we plot in Figure 2 the electronic bands for three different scenarios: (i) Vanishing spin-orbit coupling ($\xi_d = 0$) that entails $\lambda_{XR} = 0$, and sizable exchange field, $\Delta_{ex} \neq 0$, (ii) the interplay of both, finite spin-orbit and exchange interactions, and (iii) zero exchange coupling and finite spin-orbit interaction ($\lambda_{XR} \neq 0$).

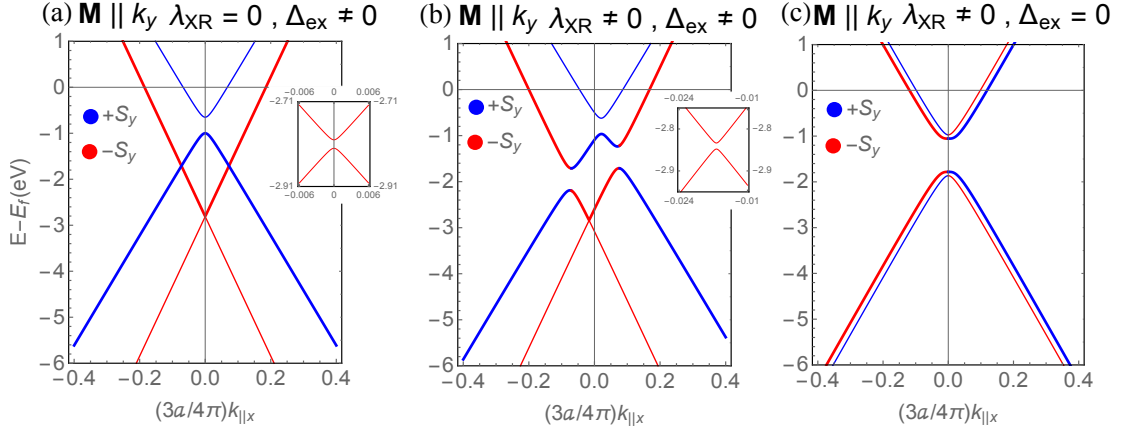


FIG. 2. Band structure in the vicinity of the Dirac point for the graphene-nickel system in the AC stacking configuration for three cases: in (a) the spin-orbit interaction of nickel is neglected and with nonzero exchange interaction, (b) both the spin-orbit interaction and the exchange (with $\xi_d \sim \Delta_{ex}$) are present, and (c) when we take into account only the spin-orbit interaction with the exchange field zero. In all the cases $k_{\parallel x}$ is the wave vector in the direction $\Gamma - K$, parallel to the graphene's plane, $p_y = 0$, $p_x = \hbar k_x - \hbar K_\xi$, and $\xi = +1$. The majority and minority spin bands are indicated with blue and red colors respectively, and the direction of the magnetization of Ni with respect to k_y is indicated. The insets (a) and (b) shows the small gap in the dispersions for the minority spin bands.

TABLE I. Parameters used to calculate the bands structure of Graphene/Ni system.

Parameter	Value	Ref.
$V_{pp\pi}$	-3.033 eV	[17],[36]
$ 2\Delta_{ex} $	0.5 eV	[25],[27],[28]
ξ_d	0.1 eV	[33]
a	2.46 Å	[36]
d	2.05 Å	[27]
$U_{pd\sigma}$	-0.651 eV	[30]
$U_{pd\pi}$	0.015 eV	[30]
Δ_0	0.401 eV	[30]
Δ_1	0.710 eV	[30]

In the first scenario ($\lambda_{XR} = 0$) the corresponding dispersion laws for the majority/minority bands follows,

$$\begin{aligned}
 E_{\pm\uparrow}(p) &= \mathcal{E}_D + \Delta_{\pm} \pm \sqrt{(\varepsilon_{+} + \Delta_{-})^2 + (v_F^* - v_d^*)^2 p^2}, \\
 E_{\pm\downarrow}(p) &= \mathcal{E}_D - \Delta_{\pm} \pm \sqrt{(\varepsilon_{+} - \Delta_{-})^2 + (v_F^* + v_d^*)^2 p^2}.
 \end{aligned}
 \tag{8}$$

where $\mathcal{E}_D = \varepsilon_{-}$, and the \pm sign in $E_{\pm,\uparrow\downarrow}$ corresponds to the electron/hole bands, respectively. In Fig. 2(a) we have plotted these bands and observe that the behavior of the dispersions for minority spin-bands (in red) preserves the linear in momentum behavior at the vicinity of the Dirac point, with a small gap of $2|\varepsilon_{+} - \Delta_{-}| = 20$ meV. These bands are symmetric with respect to the Dirac point, shifting the minority spin-bands towards lower energies by $E_{\pm\downarrow}(0) = \mathcal{E}_D - \Delta_{\pm} = -2.8$ eV, according to the

experimental value reported of ≈ 2.82 eV for graphene/Ni in the AC stacking.^{25,27} In contrast, a gap of 350 meV is opened for the majority spin-bands (in blue). This gap is governed by $|E_{+\uparrow}(0) - E_{-\uparrow}(0)| = 2|\Delta_{-} + \varepsilon_{+}|$. Also a rather large exchange spin-splitting separation between the majority hole band and the minority electron band is predicted, corresponding to an exchange energy of $|E_{-\uparrow}(0) - E_{+\downarrow}(0)| = 2|\Delta_{+} - \varepsilon_{+}| = 1.8$ eV.

Notice that we can assign a spin dependent velocity of the spin-bands, as $v_{F\uparrow(\downarrow)} = v_F^* \pm v_d^*$, that makes the velocities slightly different for the majority and the minority spin bands (see Table II). Moreover, as can be shown from Eq.(8) the term $\varepsilon_{+} \pm \Delta_{-}$ introduces in general a spin-dependent effective mass term that determines the opening of a gap between the majority/minority electron and hole bands. Since in this case we have that $\varepsilon_{+} \simeq \Delta_{-}$, (see Table II) then for the minority spin bands the gap vanishes, red lines in Fig. 2(a).

For the most general case (ii) in which the spin-orbit interaction is included and the interplay of the exchange coupling is allowed, there is no a simple analytical solution for eigenvalues of Eq. (1). In Figure 2(b) we show the numerical solution for the bandstructure for such case. The electron and hole bands become asymmetric with respect to the Dirac point, appearing large anticrossing gaps at $k_{\parallel x} \approx \pm 0.128 \text{ \AA}^{-1}$ of about 450 meV (Figure 2(b)). We can see also that the spin polarization along the y -direction $\langle S_y \rangle_{\pm}$ changes around these values of $k_{\parallel x}$ for the two adjacent bands that form the anticrossing gaps (thick lines). In Table II we show the values of the parameters used for this case. The spin-orbit induced anticrossing gap for the electron/hole ($\nu = e, h$) bands at the extremum with momentum k_m is defined

TABLE II. Estimated parameters.

Parameter	$\xi_d \sim \Delta_{ex}(\text{Ni})$	$\xi_d \ll \Delta_{ex}(\text{Co})$
ε_-	-1.8175 eV	-1.470 eV
ε_+	0.0925 eV	0.030 eV
Δ_+	0.9925 eV	1.330 eV
Δ_-	0.0825 eV	0.0298 eV
λ_{XR}	0.242 eV	0.265 eV
v_F^*	1.21×10^6 m/s	1.026×10^6 m/s
v_d^*	143196 m/s	42749 m/s
U_{p_z, z^2}^A	-0.651 eV	-0.363 eV
U_{p_z, z^2}^B	-0.268 eV	0.035 eV
$\tilde{U}_{p_z, xz}^B$	-0.767 eV	-0.538 eV
$\tilde{U}_{p_z, xy}^B$	-0.951 eV	-0.985 eV
b	0.569	0.558

as $\Delta_{so}^{(v)}(k_m) = |E_{v,+}(k_m) - E_{v,-}(k_m)|$. For the case in Figure 2(b) we have $k_m = 0.128 \text{ \AA}^{-1}$. Clearly there is an asymmetric spin-splitting as $\Delta_{so}^{(v)}(k_m) \neq \Delta_{so}^{(v)}(-k_m)$. The Dirac point for the hole-minority band is shifted to a negative value by $k_o = -0.03 \text{ \AA}^{-1}$. This asymmetry of the band structure with respect to the Dirac point, is characteristic of the joint presence of induced Rashba and exchange couplings in graphene, as reported by Rybkin *et al.*²⁶ for graphene/Au/Co. In such work the authors observed spin-orbit splittings of the order of 200 ± 40 meV at the K point, and about 40 ± 40 meV in the K' point, measurements with a reasonable agreement with their DFT calculations. Here we illustrate that a similar effect can likewise occur in graphene/Ni.

We consider now the third scenario, vanishing exchange field ($\Delta_{ex} = 0$) with finite spin-orbit interaction ($\lambda_{XR} \neq 0$) which leads also to analytical expressions for the electronic bands, $E_{c/v,s}(p) = \mathcal{E}_D \pm \mathcal{E}_s(p)$, with

$$\mathcal{E}_s(p) = \sqrt{\varepsilon_+^2 + \left(\lambda_{XR} + s \sqrt{\lambda_{XR}^2 + (v_F^* p)^2} \right)^2}, \quad (9)$$

where $\{c, v\}$ denotes the electron/hole branches, respectively, and the label $s = \pm$ refers to the spin helicity. In Figure 2(c) we plot the dispersion bands. Clearly the bands recover the symmetry with respect to the Dirac point. The sign of spin polarization S_y changes when $k_{\parallel x} \rightarrow -k_{\parallel x}$, in accordance with standard notion of Rashba spin-orbit coupling. The Rashba spin-splitting energy at $p = 0$ is thus given by $\Delta_R \equiv |\mathcal{E}_+(0) - \mathcal{E}_-(0)|$, with

$$\Delta_R = \sqrt{\varepsilon_+^2 + 4\lambda_{XR}^2} - \varepsilon_+, \quad (10)$$

leading to $\Delta_R = 82.8$ meV (see Table III). Due the p_z - d hybridization between cobalt atoms with graphene, a rather huge gap is opened between the bands with spin-chirality $s = -$, and is given by $|E_{c,-}(0) - E_{v,-}(0)| = 2|\varepsilon_+|$, corresponding to an energy of about 0.73 eV.

Figure 3 shows the same three scenarios studied in Figure 2 but neglecting the parameters Δ_- and ε_+ , which are small in magnitude in comparison to Δ_+ and ε_- ,

TABLE III. Hamiltonian parameters for $\Delta = 0$ (case $\xi_d \sim \Delta$).

Parameter	Value
ε_-	-1.428 eV
ε_+	0.373 eV
Δ_+	0
Δ_-	0
λ_{XR}	0.136 eV
v_F^*	1.126×10^6 m/s
v_d^*	0

respectively (see Table II). The main difference with respect to the results shown in Figure 2 is the closing of the gaps between the majority and the minority spin bands for the cases where it was assumed either $\lambda_{XR} \neq 0$ or $\lambda_{XR} = 0$, with $\Delta_{ex} \neq 0$ (Figure 3(a),(b)). Since ε_+ is taken equal to zero then $|E_{c,-}(0) - E_{v,-}(0)| = 0$ leading to a gapless bandstructure, Figure 3(c). For all the cases presented in Figures 2 and 3, we find that the Fermi velocities of the bands near the Dirac point ranges between 0.9×10^6 m/s and 1.1×10^6 m/s (see Tables II and III), which are very close to the experimental Fermi velocities for the intact Dirac cones reported for Graphene/Ni ($\approx 0.8 \times 10^6$ m/s^{25,27}).

The behavior of the band structure upon the inversion of the in-plane magnetization vector of the Ni layer (parallel to $-k_y$) is also studied and it is shown in Figure 4. We plot the most general scenario in which we have the joint action of the spin-orbit interaction and the exchange field (Fig. 4(a)), as well as the case in which the parameters $\Delta_- = \varepsilon_+ = 0$, Fig. 4(b). As expected, if the magnetization in nickel is inverted, the spin polarization of the graphene bands is likewise inverted. The asymmetries of the bands with respect to the Dirac point become also the mirror images with respect to the magnetization parallel to $+k_y$.

D. Low Energy Dispersion for Graphene/Co

Interestingly, our Slater-Koster tight-binding model offers an explanation for the appearance of intact and gapless Dirac cones formed by the minority spin bands in graphene on cobalt, as observed recently through spin- and angle-resolved photoemission measurements.^{25,27,28} We notice that the preservation of the linearity of the spin-bands together with a gapless (or nearly gapless) regime occurs whenever the atomic spin-orbit coupling is much smaller than the exchange field ($\xi_d \ll \Delta_{ex}$) as for the case of graphene/Co (Table IV). In Figure 5(a) we plot the resulting band structure for graphene/Co. We observe that the minority spin bands show a linear dispersion at the vicinity of the K point with a rather small gap $\lesssim 1$ meV, in contrast with the case of graphene/Ni where $\xi_d \sim \Delta_{ex}$ and a gap of about 20 meV is obtained. The smallness of such gap in

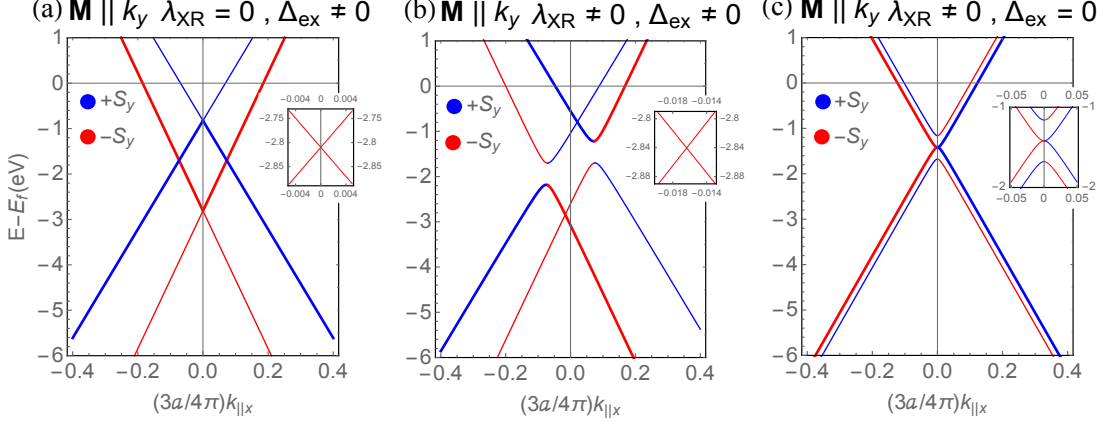


FIG. 3. Band structure in the vicinity of the K point as a function of $k_{\parallel x}$ with $k_y = 0$ for the graphene/Ni neglecting the small parameters Δ_- and ε_+ . We show here the same three cases of Fig. 2: (a) finite exchange coupling in the absence of the spin-orbit interaction of the Ni-atoms, (b) when both, the spin orbit interaction and the exchange are present, and (c) with spin-orbit interaction present whiles and the exchange field is set to zero. The insets show the absence of gaps between the bands in (b) and the Rashba splitting in (c).

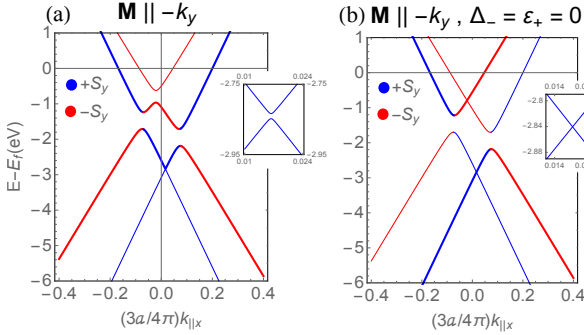


FIG. 4. (Band structure in the vicinity of the Dirac point for the graphene-cobalt with inverted magnetization respect to Figure 3 for: (a) when we take the parameters Δ_- and ε_+ , (b) when we neglect the parameters Δ_- and ε_+ . In both the cases $k_{\parallel x}$ is the wave vector in the direction $\Gamma - K$, parallel to the graphene's plane, $p_y = 0$, $p_x = \hbar k_x - \hbar K \xi$, and $\xi = +1$. The majority and minority spin bands are indicated with blue and red colors respectively, and the direction of the magnetization of Co with respect to k_y is indicated. The insets show the gaps between the bands in (a) and the absence of gaps in (b).

graphene/Co turns to be much smaller than the precision of the SARPES experimental reports on gapless intact Dirac cones.^{25,27,28} We may presume that such tiny gap predicted here was actually present in these experiments, but very likely passed unnoticed due their lack of resolution for such small range of energies and the broadening of the bands. We also observe that the asymmetry generated by the spin-orbit interaction is not as pronounced as in the $\xi_d \sim \Delta_{ex}$ case. Here the horizontal uniform asymmetric momentum shifting of the bands is also of the order $(3a/4\pi)k_{\parallel x} = 0.02$. Notice that the model

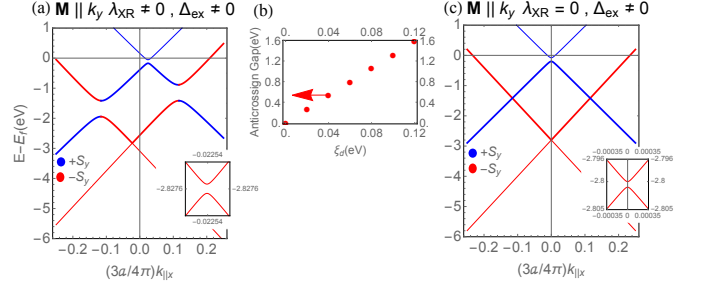


FIG. 5. (a): Band structure in the vicinity of the Dirac point with $k_y = 0$ for the graphene-cobalt system in the AC stacking configuration, for the case in which the spin-orbit interaction of cobalt is included. As before, k_{\parallel} is the wave vector in the direction $\Gamma - K$, parallel to the graphene's plane. The majority and minority spin bands are indicated with blue and red colors respectively. (b) Plot of the anti-crossing gap in function of the tight-binding spin-orbit parameter ξ_d . (c) same as (a) but neglecting the spin-orbit coupling.

also predicts the opening of a rather large anticrossing gaps between the majority and minority spin bands (~ 0.510 eV), here occurring at approximately $\pm 0.19 \text{ \AA}^{-1}$. Such gaps were not reported in the experimental bands for Graphene/Co(0001)^{25,27,28}, perhaps due the fact that these bands were not clearly resolved in the experiment below the Dirac point due to the strong hybridization of the π bands of graphene with the $3d$ bands of cobalt. We can trace-back the origin of this effect to the induced magneto-spin-orbit Rashba type term in the low energy effective Hamiltonian (Eq. (1)) and governed by the strength of λ_{XR} . In Figure 5(b) we depict the linear relationship between these anticrossing gaps and the intrinsic spin-orbit parameter ξ_d of cobalt. The open-

TABLE IV. Parameters used to calculate the bands structure of Graphene/Co system

Parameter	Value	Ref.
$V_{pp\pi}$	-3.033 eV	[17],[36]
$ 2\Delta_{ex} $	1.6 eV	[25],[27],[28]
ξ_d	0.04 eV	[33]
a	2.46 Å	[36]
d	2.11 Å	[27]
$U_{pd\sigma}$	-0.126 eV	[30]
$U_{pd\pi}$	0.286 eV	[30]
Δ_0	-0.794 eV	[30]
Δ_1	1.246 eV	[30]

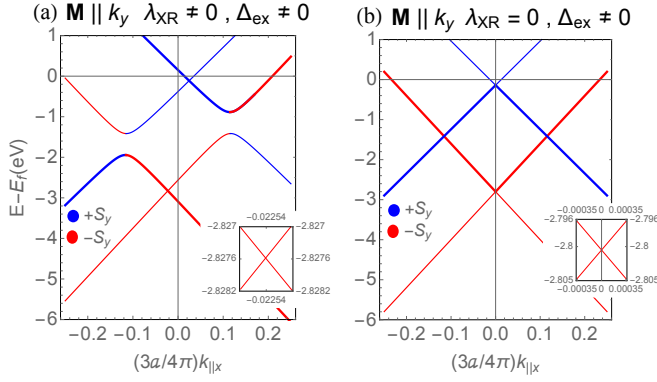


FIG. 6. Bands structure in the vicinity of the Dirac point for the graphene-cobalt system in the AC stacking configuration: (a) neglecting the parameters ε_+ and Δ_- , and (b) **same as (a)**, **but** for the case in which the spin orbit interaction of cobalt is not included. In both plots $k_{||}$ is the wave vector in the direction $\Gamma - K$, parallel to the graphene's plane. In these plots we took $p_y = 0$, $p_x = \hbar k_x - \hbar K_\xi$, and $\xi = +1$. The majority and minority spin bands are indicated with blue and red colors respectively.

ing of such gaps arises clearly as long as $\xi_d \sim \Delta_{ex}$, exhibiting closing gaps for the physical condition for which $\xi_d \ll \Delta_{ex}$. The effect of neglecting the λ_{XR} contribution leading to vanishing anticrossing gaps far away from the Dirac point is shown in Figure 5(c).

In order to further illustrate the strong influence in the anticrossing effect of the cobalt spin-orbit coupling ξ_d as well as the sensitivity of the parameters on the band structure, we plot in Figure 6 the bands for the system graphene/cobalt in the limit $\varepsilon = 0$ and $\Delta_- = 0$, for two cases: Figure 6(a) with a nonzero spin-orbit interaction term (thereby $\lambda_{XR} \neq 0$), and in Figure 6(b) when the spin-orbit coupling is totally absent (Figure 6(b)) but maintaining the rest of the parameters as in the case $\xi_d \ll \Delta_{ex}$ (Table IV). The closing of the gap at $(4\pi/3a)k_{||,x} \simeq 0.1$ by making $\xi_d = 0$ is evident (Figure 6(b)). Interestingly under this conditions a gapless

intact Dirac cone is formed by the minority spin bands with its apex shifted by $E_{\pm\downarrow}(0) = \mathcal{E}_D - \Delta_+ = -2.8$ eV. The effective masses associated to the spin- dispersions laws of Eq.(8) are dictated by

$$\frac{1}{m_{\pm\uparrow,\downarrow}^*} = \pm \frac{(v_{F\uparrow,\downarrow}^*)^2}{\varepsilon_+ \pm \Delta_-}, \quad (11)$$

where explicitly in terms of the Slater-Koster parameters we have

$$\varepsilon_+ \pm \Delta_- = \frac{3b^2 (\tilde{U}_{p_z,xz}^B)^2 + \frac{1}{4}b^2 (\tilde{U}_{p_z,xy}^B)^2}{2 (\Delta_1 \pm \Delta_{ex})} + \frac{3 (U_{p_z,z^2}^B)^2 - \frac{1}{3}(U_{p_z,z^2}^A)^2}{2 (\Delta_0 \pm \Delta_{ex})}, \quad (12)$$

which gives insight to the type of Co-graphene hybridizations that determines the breaking of the Dirac cones and the appearing of parabolic bands, as well as the criteria for the preservation of massless Dirac Fermions for the spin-minority bands. For instance, vanishing effective mass for the spin-minority bands entails $(\varepsilon_+ - \Delta_-) \rightarrow 0$, physical situation occurring in Fig. (6). Indeed, we can corroborate from Eq. (12) and Table II that the first term to the right basically cancels the second term, producing massless intact Dirac cones. It is worth noticing that due the p - d orbital overlapping in combination with the exchange field, the Fermi velocities become renormalized such that the velocity v_{\downarrow}^* for the spin minority linear bands becomes reduced respect to the free-standing graphene v_F .

III. CONCLUSIONS

We investigated theoretically the proximity effects induced in a monolayer of graphene over a monolayer of a ferromagnetic metal Ni and Co within the Slater-Koster approximation in a multi-orbital tight-binding approach. We construct a minimal model that includes the spin-orbit coupling and the exchange fields of the ferromagnetic atoms, besides the hybridizations of the $3d$ -orbitals of Ni(Co) atoms with those of graphene's p_z -orbitals. From this, we derive a low energy effective Hamiltonian that dictates the dispersion laws for graphene/Ni(Co) which is consistent with recent DFT calculations and with photoemission experiments with spin-resolution.

The low energy Hamiltonian contains three dominant terms: an effective Dirac term with a perturbed velocity shifted by an exchange field dependent velocity. The second term has formally the structure of a Rashba type spin-orbit interaction, transferred to graphene from the intrinsic spin-orbit of nickel(cobalt) and from the overlaps between the A(B) p_z orbitals of graphene with the d_{z^2} (d_{xz} and d_{yz}) of the ferromagnetic atoms. Finally the

third term has the form of a constant matrix that mostly depends on the exchange fields.

As a consequence of the nature of these terms in the effective Hamiltonian, the first which is linear in momentum, produces spin-asymmetric bands with respect to $k_{\parallel x} = 0$ with reduced Fermi velocities. Then the joint action of the Rashba-type and exchange terms induces a magneto-spin-orbit effect on the spin bands, leading to large asymmetries between the minority(majority) spin bands and the appearance of gaps at the Dirac point and to anticrossing-gaps away from it.

We illustrated two regimes. In the first, the spin orbit coupling is similar to the exchange coupling ($\xi_d \sim \Delta_{ex}$). This situation physically corresponds to the system of graphene/Ni in the AC stacking configuration. We showed that the band structure for this system presents the combination of a strong exchange and Rashba coupling, known as the Rashba+Exchange effect.²⁶ This description is given in terms of the overlaps between orbitals, the exchange coupling and the atomic spin orbit parameter of nickel. The second regime corresponds to the case in which the spin orbit coupling is much smaller than the exchange coupling ($\xi_d \ll \Delta_{ex}$). This scenario occurs in the system of graphene/Co in the AC stacking configuration. For this system, we were able to give an insight on the experimentally observed intact Dirac cones.^{25,27,28} In this sense, we noticed that this effect is produced because the spin dependent effective mass term, which depends on the graphene-cobalt hybridizations, goes to zero for the minority spin bands. In summary, we have shown that proximity effects emerging from depositing graphene on a ferromagnetic metal substrate such as nickel and cobalt can change significantly the dynamics of its Dirac electronic states, inducing very large exchange fields and giant spin-orbit coupling to the graphene layer comprising a magneto-spin-orbit effect and intact Dirac bands which may be of great interest for spintronics applications.

ACKNOWLEDGMENTS

M. P. acknowledges the use of the facilities of the Center of Nanosciences and Nanotechnology (CNyN) of the National Autonomous University of Mexico, as well as to the National Council for Science and Technology of Mexico (CONACyT) and to the Mexican ministry of energy (SER) for providing a post-doctoral fellowship to carry out this research.

Appendix A: Tight-binding approach

In the absence of spin-orbit and exchange interactions the Hamiltonian for graphene/Ni(Co) interface in real

space reads

$$\hat{H}_{TB} = -\frac{\hbar^2}{2m}\nabla^2 + \sum_i V_C(\mathbf{r}-\mathbf{R}_i^C) + \sum_{i'} V_{Ni(Co)}(\mathbf{r}-\mathbf{R}_{i'}^{Ni(Co)}), \quad (\text{A1})$$

where the first term corresponds to the kinetic energy of the electrons and the second/third terms to the atomic potential $V_{C/Ni(Co)}$ of carbon/nickel(cobalt) ions, which in the two center approximation, only involves the atoms i/i' at the vector positions $\mathbf{R}_i^C/\mathbf{R}_{i'}^{Ni(Co)}$ and its first neighbors, respectively. We are interested in the matrix elements of \hat{H}_{TB} in the subspace spanned by the $2p_z$ orbitals for the two distinct A and B sites of graphene with states $|p_{z,s}^{A/B}\rangle$ and in the subspace spanned by the $3d$ -orbitals of Ni(Co) (only at sites A), that is, the states $|\phi_\mu\rangle \otimes |s\rangle$, where $\mu = \{1, 2, 3, 4, 5\}$ denotes the five $3d$ -orbitals of cobalt, and $s = \{\uparrow, \downarrow\}$ labels the electron spin. The Wannier functions centered on the different atomic sites are assumed to be orthogonal. Hence the Slater-Koster Hamiltonian matrix elements are $\langle\varphi_{\mu,s}|\hat{H}_{TB}|\varphi_{\mu',s'}\rangle$, with $\{|\varphi_{\mu,s}\rangle\} = \{|p_{z,s}^A\rangle, |p_{z,s}^B\rangle, |\phi_{\mu,s}\rangle\}$. This generates a 14×14 overlapping matrix for the graphene/Ni(Co) interface,

$$H_o = \begin{pmatrix} H_\pi & U \\ U^\dagger & \mathcal{E}_{Ni(Co)} \end{pmatrix} \otimes \{|\uparrow, \downarrow\rangle\}, \quad (\text{A2})$$

where H_π is the bare graphene Hamiltonian matrix in the basis $\{|p_z^A, p_z^B\rangle\} \otimes \{|\uparrow, \downarrow\rangle\}$, having the form

$$H_\pi = \begin{pmatrix} 0 & V_{pp\pi} \\ V_{pp\pi} & 0 \end{pmatrix}, \quad (\text{A3})$$

and the on-site energy of the $2p$ orbitals of graphene, $\varepsilon_p = \langle p_{z,s}^{A/B}|\hat{H}_{TB}|p_{z,s}^{A/B}\rangle = 0$, has been chosen as the reference energy. Here $V_{pp\pi}$ is the Slater-Koster parameter for the overlaps between p_z carbon orbitals when they form pure π -bondings.³⁵

On the other hand, for the Ni(Co)-atoms there is a natural breaking of the degeneracies of the $3d$ -orbital states due to the crystal field. Hence, in the absence of magnetic fields, such that time reversal symmetry is satisfied, the five $3d$ -orbitals of Ni(Co) split into three spin degenerate groups: two doublets E_1 (with $3d_{xz}$ and $3d_{yz}$ orbitals) and E_2 (with d_{xy} and $3d_{x^2-y^2}$ orbitals) and a singlet A_1 (consisting only of $3d_{z^2-r^2}$ orbitals).³¹ In the basis $\{|\phi_\nu\rangle\} = \{d_{xz}, d_{yz}, d_{3z^2-r^2}, d_{xy}, d_{x^2-y^2}\}$, the on-site matrix elements for the Ni(Co)-atoms with respect to the on-site energy ε_p of the p orbitals of graphene is given by

$$\mathcal{E}_{Ni(Co)} = \begin{pmatrix} \varepsilon_{d_1} - \varepsilon_p & 0 & 0 & 0 & 0 \\ 0 & \varepsilon_{d_1} - \varepsilon_p & 0 & 0 & 0 \\ 0 & 0 & \varepsilon_{d_0} - \varepsilon_p & 0 & 0 \\ 0 & 0 & 0 & \varepsilon_{d_2} - \varepsilon_p & 0 \\ 0 & 0 & 0 & 0 & \varepsilon_{d_2} - \varepsilon_p \end{pmatrix}, \quad (\text{A4})$$

where the label $d_{|m|}$ correspond to the $m = 0, \pm 1, \pm 2$ magnetic orbital states of the on-site energies $\varepsilon_{d_{|m|}}$. Here we are assuming that the energetically favorable configuration is that with Ni(Co)-atoms lying directly underneath the graphene sublattice A . Therefore, it is expected that the $3d_{3z^2-r^2}$ orbitals of the A_1 group (referred now on as d_{z^2} orbitals) will hybridizes strongly with p_z orbitals of the sublattice A carbon atoms. By the same token, the Ni(Co)-atoms of the $E_{1,2}$ group symmetry containing the orbitals $d_{\{xz,yz,xy,x^2-y^2\}}$ will not hybridize with carbon atoms of the A sublattice, but only with the sublattice B . Given the marked differences between the hybridization of these two groups of orbitals, here we shall assume that the onsite energies are

renormalized by the proximity with graphene such that $\varepsilon_{d_2} \simeq \varepsilon_{d_1}$ ²⁷.

The graphene-nickel(cobalt) overlapping matrix U , reads

$$U(\hat{\tau}_j) = \begin{pmatrix} U_{p_z,xz}^A & U_{p_z,yz}^A & U_{p_z,z^2}^A & U_{p_z,xy}^A & U_{p_z,x^2}^A \\ U_{p_z,xz}^B & U_{p_z,yz}^B & U_{p_z,z^2}^B & U_{p_z,xy}^B & U_{p_z,x^2}^B \end{pmatrix}, \quad (\text{A5})$$

where the matrix elements $U_{p_z,\nu}^{A/B} \equiv \langle p_{z,s}^{A/B} | \hat{H}_{TB} | \phi_{\nu,s}^{Ni(Co)} \rangle$ depend explicitly on the Slater-Koster parameters $V_{pd\sigma}$ and $V_{pd\pi}$ corresponding to overlaps between carbon p_z orbitals and nickel(cobalt) d orbitals, and the cosine directors joining these atoms (see Fig. (7)).

$$\begin{aligned} U_{p_z,z^2}^{A/B} &= \langle p_{z,s}^{A/B} | \hat{H}_{TB} | d_{3z^2-r^2,s} \rangle = \sqrt{3}m_z(m_x^2 + m_y^2)U_{pd\pi} - \frac{1}{2}m_z(m_x^2 + m_y^2 - 2m_z^2)U_{pd\sigma} \\ U_{p_z,x^2}^{A/B} &= \langle p_{z,\sigma_s}^{A/B} | \hat{H}_{TB} | d_{x^2-y^2,s} \rangle = \frac{\sqrt{3}}{2}m_z(m_x^2 - m_y^2)U_{pd\sigma} - m_z(m_x^2 - m_y^2)U_{pd\pi} \\ U_{p_z,\{x,y\}z}^{A/B} &= \langle p_{z,s}^{A/B} | \hat{H}_{TB} | d_{\{x,y\}z,s} \rangle = \sqrt{3}m_z^2m_{\{x,y\}}U_{pd\sigma} + (1 - 2m_z^2)m_{\{x,y\}}U_{pd\pi} \\ U_{p_z,xy}^{A/B} &= \langle p_{z,s}^{A/B} | \hat{H}_{TB} | d_{xy,s} \rangle = m_zm_xm_y(\sqrt{3}U_{pd\sigma} - 2U_{pd\pi}). \end{aligned} \quad (\text{A6})$$

where, for simplicity we have dropped the site j -index, and the components of the unit vector $\mathbf{m} = (m_x, m_y, m_z)$, are $m_l = \{\nu_l, \mu_l\}$ specified by the cosine directors between the carbon atoms at $\{A, B\}$ to the nearby nickel(cobalt) atom, respectively, with $l = \{x, y, z\}$. Note that in the AC stacking configuration chosen here, the overlapping between the graphene atoms of sublattice A and Ni(Co) are all zero from symmetry ($\nu_x = \nu_y = 0$, and $\nu_z = -1$), with the sole exception of the atomic p_z orbitals coupling the $d_{3z^2-r^2}$ -orbitals, namely $U_{p_z,z^2}^A \equiv U_{pd\sigma}$. For carbon atoms in sublattice B we have $U_{p_z,xz}^B = \mu_{jx}\tilde{U}_{p_z,xz}^B$, $U_{p_z,yz}^B = \mu_{jy}\tilde{U}_{p_z,xz}^B$, $U_{p_z,xy}^B = \mu_{jx}\mu_{jy}\tilde{U}_{p_z,xy}^B$, and $U_{p_z,x^2}^B = \frac{1}{2}(\mu_{jx}^2 - \mu_{jy}^2)\tilde{U}_{p_z,xy}^B$. With the matrix elements

$$\tilde{U}_{p_z,xz}^B = \sqrt{3}\mu_z^2U_{pd\sigma} + (1 - 2\mu_z^2)U_{pd\pi} \quad (\text{A7})$$

$$\tilde{U}_{p_z,xy}^B = \mu_z(\sqrt{3}U_{pd\sigma} - 2U_{pd\pi}). \quad (\text{A8})$$

where $U_{pd\sigma}$ and $U_{pd\pi}$ are the Slater-Koster parameters corresponding to overlaps between graphene p_z and nickel(cobalt) d -orbitals that can be fitted to first principal calculations.

1. Atomic spin-orbit interaction

The dominant intrinsic spin-orbit interaction in the graphene/Ni(Co) interface will arise among the outer shell d -orbitals of nickel(cobalt). Spin-orbit interaction of carbon atoms and between different atoms are assumed

to be negligible. The local spin-orbit interaction is modeled through the term,^{17,18}

$$H_{so} = \frac{\hbar}{2m^2c^2} (\nabla V(\mathbf{r}) \times \mathbf{p}) \cdot \mathbf{s} = \xi(r)\mathbf{L} \cdot \mathbf{S}, \quad (\text{A9})$$

where m is the free electron mass, c is the speed of light, $V(\mathbf{r})$ is the potential of the nickel(cobalt) ions, \mathbf{p} is the linear momentum operator, $\mathbf{s} = (s_x, s_y, s_z)$ with s_i , $i = \{x, y, z\}$ the standard Pauli matrices, $\mathbf{S} = \frac{\hbar}{2}\mathbf{s}$ is the electron spin vector operator, and \mathbf{L} is the orbital angular momentum operator. Within the two center approximation the atomic potential is deem to be spherical symmetric, $V(\mathbf{r}) \rightarrow V(r)$, then $\nabla V(r) = \hat{r}dV/dr$. Hence the function

$$\xi(r) = \frac{\hbar}{2m^2c^2} \frac{1}{r} \frac{dV}{dr} \quad (\text{A10})$$

contains all the radial dependence. We are interested in the the matrix elements

$$\langle \phi_{\nu,s}^{Ni(Co)} | H_{so} | \phi_{\nu',s'}^{Ni(Co)} \rangle = \langle \phi_{\nu,s}^{Ni(Co)} | \xi(r)\mathbf{L} \cdot \mathbf{S} | \phi_{\nu',s'}^{Ni(Co)} \rangle \quad (\text{A11})$$

by writing $\{|\phi_{\nu,s}^{Ni(Co)}\rangle\}$ in the basis of the eigenkets of the angular momentum $\{|l, m\rangle\}$, with $l = 2$ and $m = 0, \pm 1, \pm 2$ spanning all the $3d$ -orbitals of nickel(cobalt), matrix elements of the form $\xi_l(l, m | \mathbf{L} \cdot \mathbf{S} | l', m') \delta_{l,\nu}$ has to be calculated in which $\xi_l = \int_0^\infty \xi(r)R_l^2(r)r^2dr$ is the intrinsic spin-orbit coupling parameter, where R_l is the unknown radial wave function for nickel(cobalt) atoms. For $l = 2$ we use the notation $\xi_{l=2} \rightarrow \xi_d$. Because the explicit form of Eq. (A10) neither $R_l(r)$ are known, the value of

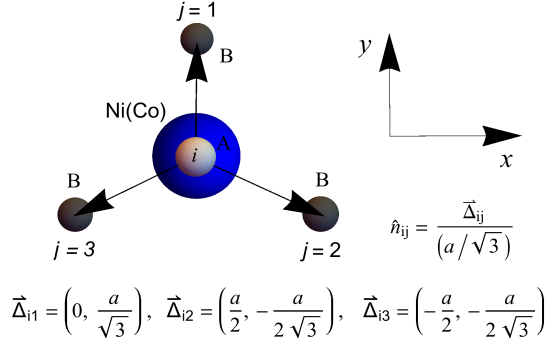


FIG. 7. Scheme that shows the cosine directors to first neighbors, from atoms at A sublattice to atoms to B sublattice in the graphene plane, n_{ij} . The cosine directors from the i -th carbon atom at A to the nearby nickel(cobalt) atom are, $\nu_{ix} = 0$, $\nu_{iy} = 0$ and $\nu_{iz} = -1$; while the cosine directors from nearest neighbor $j = 1, 2, 3$ carbon atoms at B to the nickel(cobalt) atom are defined by $\mu_{jx} = -bn_{ijx}$, $\mu_{jy} = -bn_{ijy}$ and $\mu_{jz} = d/\zeta$, where $b = (a/\sqrt{3})/\zeta$, with $\zeta = \sqrt{(a/\sqrt{3})^2 + d^2}$, (not shown). Here the graphene lattice parameter $a = 2.46\text{\AA}$, and the graphene-Ni(Co) distance is d .

$$H_{so}^{Ni(Co)} = \begin{pmatrix} 0 & 0 & -i\xi_d & 0 & 0 & \sqrt{3}\xi_d & 0 & i\xi_d & 0 & -\xi_d \\ 0 & 0 & 0 & i\xi_d & -\sqrt{3}\xi_d & 0 & i\xi_d & 0 & \xi_d & 0 \\ i\xi_d & 0 & 0 & 0 & 0 & -i\sqrt{3}\xi_d & 0 & -\xi_d & 0 & -i\xi_d \\ 0 & -i\xi_d & 0 & 0 & -i\sqrt{3}\xi_d & 0 & \xi_d & 0 & -i\xi_d & 0 \\ 0 & -\sqrt{3}\xi_d & 0 & i\sqrt{3}\xi_d & 0 & 0 & 0 & 0 & 0 & 0 \\ \sqrt{3}\xi_d & 0 & i\sqrt{3}\xi_d & 0 & 0 & 0 & 0 & 0 & 0 & 0 \\ 0 & -i\xi_d & 0 & \xi_d & 0 & 0 & 0 & 0 & 2i\xi_d & 0 \\ -i\xi_d & 0 & -\xi_d & 0 & 0 & 0 & 0 & 0 & 0 & -2i\xi_d \\ 0 & \xi_d & 0 & i\xi_d & 0 & 0 & -2i\xi_d & 0 & 0 & 0 \\ -\xi_d & 0 & i\xi_d & 0 & 0 & 0 & 0 & 2i\xi_d & 0 & 0 \end{pmatrix}. \quad (\text{A12})$$

2. Exchange field coupling

When graphene is put in proximity with a ferromagnetic layer its electrons experiences an exchange field that leads to the breaking the time reversal symmetry of its bandstructure. Such induced exchange field occurs due to quantum virtual hopping between the graphene layer and the ferromagnetic atoms, removing the degeneracy of the spins states. Thus for collinear ferromagnetic states, spin electrons with up/down orientations (majority/minority spin bands) will experience different energies depending whether their spin is parallel/antiparallel to the local magnetic moment of the ferromagnetic atoms. In what follows we will adopt a simple tight-binding Stoner Hamiltonian³² that models the electron spin splitting through a local (on-site) potential energy.

The tight-binding Stoner model depends on the local

ξ_d has to be determined from DFT calculations. In this paper we use $\xi_d = 0.11$ eV for nickel and $\xi_d = 0.04$ eV for cobalt, which are similar to the values presented in Table IV.³³

Finally the full 10×10 matrix that describes the spin-orbit interaction in the extended basis $\{d_{xz,\uparrow}, d_{xz,\downarrow}, d_{yz,\uparrow}, d_{yz,\downarrow}, d_{3z^2-r^2,\uparrow}, d_{3z^2-r^2,\downarrow}, d_{xy,\uparrow}, d_{xy,\downarrow}, d_{x^2-y^2,\uparrow}, d_{x^2-y^2,\downarrow}\}$ is given by,

magnetization $\mathbf{M}_{i,d}$ = of atom i summed over the orbitals of character d since in transition metals the magnetization is mainly carried out by the $3d$ -orbitals. In spin-space the Stoner potential has the form³³

$$\mathbf{V}_i^{\text{Stoner}} = -\frac{1}{2}I_{i,d}(\mathbf{M}_{i,d} \cdot \mathbf{s}) \quad (\text{A13})$$

where I_i is the Stoner parameter for the atom i , and \mathbf{s} is the vector of the spin Pauli matrices. In this work we chose the magnetization the ferromagnetic nickel(cobalt) layer to be along the y -axis, $\mathbf{M} = M\hat{y}$, thus the Hamiltonian describing the induced exchange field arisen due to the d -orbitals of the ferromagnetic layer in the spin-space is parametrized as follows

$$\mathcal{H}_{ex} = \Delta_{ex}s_y \quad (\text{A14})$$

where the exchange splitting energy $\Delta_{ex} = |2\Delta_o|$ with

$\Delta_o = -\frac{1}{2}I_{i,d}M_{i,d}$, in particular the splitting energy $\Delta_o = 0.25$ eV for nickel and $\Delta_o = 0.8$ eV for cobalt atoms.³³

$$\mathcal{H}_{ex} = \begin{pmatrix} 0 & -i\Delta_{ex} & 0 & 0 & 0 & 0 & 0 & 0 & 0 & 0 \\ i\Delta_{ex} & 0 & 0 & 0 & 0 & 0 & 0 & 0 & 0 & 0 \\ 0 & 0 & 0 & -i\Delta_{ex} & 0 & 0 & 0 & 0 & 0 & 0 \\ 0 & 0 & i\Delta_{ex} & 0 & 0 & 0 & 0 & 0 & 0 & 0 \\ 0 & 0 & 0 & 0 & 0 & -i\Delta_{ex} & 0 & 0 & 0 & 0 \\ & 0 & 0 & 0 & i\Delta_{ex} & 0 & 0 & 0 & 0 & 0 \\ 0 & 0 & 0 & 0 & 0 & 0 & 0 & -i\Delta_{ex} & 0 & 0 \\ 0 & 0 & 0 & 0 & 0 & 0 & i\Delta_{ex} & 0 & 0 & 0 \\ 0 & 0 & 0 & 0 & 0 & 0 & 0 & 0 & 0 & -i\Delta_{ex} \\ 0 & 0 & 0 & 0 & 0 & 0 & 0 & 0 & i\Delta_{ex} & 0 \end{pmatrix}, \quad (\text{A15})$$

3. Full tight-binding Hamiltonian

Taking into account the spin-orbit and exchange interactions in the full Hamiltonian for graphene/Ni(Co) interface we find

$$\mathcal{H} = \begin{pmatrix} \mathcal{H}_\pi & \mathcal{U} \\ \mathcal{U}^\dagger & \mathcal{H}_\chi \end{pmatrix}, \quad (\text{A16})$$

where

$$\mathcal{H}_\pi = H_\pi \otimes \{|\uparrow, \downarrow\rangle\} \quad (\text{A17})$$

specifies the freestanding graphene π -bands, the graphene-nickel(cobalt) coupling part is given by

$$\mathcal{U} = U \otimes \{|\uparrow, \downarrow\rangle\}, \quad (\text{A18})$$

and $\mathcal{H}_\chi = E_{Ni(Co)} + H_{so}^{Ni(Co)} + H_{ex}$, with $E_{Ni(Co)} = \mathcal{E}_{Ni(Co)} \otimes \{|\uparrow, \downarrow\rangle\}$ incorporates the one-site, spin-orbit and exchange field contribution of the Ni(Co) atoms. Explicitly, In the extended basis $\{d_{xz,\uparrow}, d_{xz,\downarrow}, d_{yz,\uparrow}, d_{yz,\downarrow}, d_{3z^2-r^2,\uparrow}, d_{3z^2-r^2,\downarrow}, d_{xy,\uparrow}, d_{xy,\downarrow}, d_{x^2-y^2,\uparrow}, d_{x^2-y^2,\downarrow}\}$, the matrix \mathcal{H}_χ has the form,

$$\mathcal{H}_\chi = \begin{pmatrix} \varepsilon_{d_1} - \varepsilon_p & -i\Delta_{ex} & -i\xi_d & 0 & 0 & \sqrt{3}\xi_d & 0 & i\xi_d & 0 & -\xi_d \\ i\Delta_{ex} & \varepsilon_{d_1} - \varepsilon_p & 0 & i\xi_d & -\sqrt{3}\xi_d & 0 & i\xi_d & 0 & \xi_d & 0 \\ i\xi_d & 0 & \varepsilon_{d_1} - \varepsilon_p & -i\Delta_{ex} & 0 & -i\sqrt{3}\xi_d & 0 & -\xi_d & 0 & -i\xi_d \\ 0 & -i\xi_d & i\Delta_{ex} & \varepsilon_{d_1} - \varepsilon_p & -i\sqrt{3}\xi_d & 0 & \xi_d & 0 & -i\xi_d & 0 \\ 0 & -\sqrt{3}\xi_d & 0 & i\sqrt{3}\xi_d & \varepsilon_{d_o} - \varepsilon_p & -i\Delta_{ex} & 0 & 0 & 0 & 0 \\ \sqrt{3}\xi_d & 0 & i\sqrt{3}\xi_d & 0 & i\Delta_{ex} & \varepsilon_{d_o} - \varepsilon_p & 0 & 0 & 0 & 0 \\ 0 & -i\xi_d & 0 & \xi_d & 0 & 0 & \varepsilon_{d_2} - \varepsilon_p & -i\Delta_{ex} & 2i\xi_d & 0 \\ -i\xi_d & 0 & -\xi_d & 0 & 0 & 0 & i\Delta_{ex} & \varepsilon_{d_2} - \varepsilon_p & 0 & -2i\xi_d \\ 0 & \xi_d & 0 & i\xi_d & 0 & 0 & -2i\xi_d & 0 & \varepsilon_{d_2} - \varepsilon_p & -i\Delta_{ex} \\ -\xi_d & 0 & i\xi_d & 0 & 0 & 0 & 0 & 2i\xi_d & i\Delta_{ex} & \varepsilon_{d_2} - \varepsilon_p \end{pmatrix}. \quad (\text{A19})$$

Appendix B: Effective Low-Energy Hamiltonian

We use the standard band folding method to find the low-energy Hamiltonian of graphene/Ni(Co) system and focus our attention to the modifications of the π -bands associated to \mathcal{H}_π due the rest of the interactions. For this we require that eigenvalues $\langle \mathcal{H}_\chi \rangle \ll \langle \mathcal{H}_\pi \rangle$, and that the characteristic energies $\langle \mathcal{U} \rangle \ll (\langle \mathcal{H}_\chi \rangle - \langle \mathcal{H}_\pi \rangle)$. The eigenvalue equation for the full Hamiltonian Eq. (A16) is

$$\begin{pmatrix} \mathcal{H}_\pi & \mathcal{U} \\ \mathcal{U}^\dagger & \mathcal{H}_\chi \end{pmatrix} \begin{pmatrix} G \\ \chi \end{pmatrix} = E \begin{pmatrix} G \\ \chi \end{pmatrix}, \quad (\text{B1})$$

where $G = \{\psi_{p_z\uparrow}^A, \psi_{p_z\downarrow}^A, \psi_{p_z\uparrow}^B, \psi_{p_z\downarrow}^B\}$, and $\chi = \{\psi_{d_{xz,\uparrow}}, \psi_{d_{xz,\downarrow}}, \psi_{d_{yz,\uparrow}}, \psi_{d_{yz,\downarrow}}, \psi_{d_{3z^2-r^2,\uparrow}}, \psi_{d_{3z^2-r^2,\downarrow}}, \psi_{d_{xy,\uparrow}}, \psi_{d_{xy,\downarrow}}, \psi_{d_{x^2-y^2,\uparrow}}, \psi_{d_{x^2-y^2,\downarrow}}\}$ are the wave functions in the graphene and nickel(cobalt) subspace, respectively. The elimination of χ from Eq. (B1) gives:

$$[\mathcal{H}_\pi + \mathcal{U}(E - \mathcal{H}_\chi)^{-1}\mathcal{U}^\dagger]G = EG, \quad (\text{B2})$$

and expanding $(E - \mathcal{H}_\chi)^{-1}$ up to first order in E , we obtain $[\mathcal{H}_\pi - \mathcal{U}\mathcal{H}_\chi^{-1}\mathcal{U}^\dagger]G \approx ESG$, where $S = 1 + \mathcal{U}\mathcal{H}_\chi^{-2}\mathcal{U}^\dagger$. By defining $\Phi = S^{1/2}G$, normalized to $|\Phi|^2 \approx G^\dagger G + \chi^\dagger \chi$ to the same order as the new effective Hamiltonian, we get

$$S^{-1/2}[\mathcal{H}_\pi - \mathcal{U}\mathcal{H}_\chi^{-1}\mathcal{U}^\dagger]S^{-1/2}\Phi = \mathcal{H}_{\text{eff}}\Phi \simeq E\Phi. \quad (\text{B3})$$

Therefore, after using Eqs. (A17),(A18) and (A19); and going to the reciprocal space by using the cosine directors of Figure 7, the effective low-energy Hamiltonian for graphene perturbed by its interaction with nickel(cobalt) has the form (assuming $S \approx 1$)

$$\mathcal{H}_{\text{eff}}(\mathbf{p}) \simeq \mathcal{H}_\pi - \mathcal{U}\mathcal{H}_\chi^{-1}\mathcal{U}^\dagger = \begin{pmatrix} \varepsilon_+ + \varepsilon_- & 0 & v_F^* p_- & i v_d^* p_- \\ 0 & \varepsilon_+ + \varepsilon_- & -i v_d^* p_- & v_F^* p_- \\ v_F^* p_+ & i v_d^* p_+ & \varepsilon_- - \varepsilon_+ & 0 \\ -i v_d^* p_+ & v_F^* p_+ & 0 & \varepsilon_- - \varepsilon_+ \end{pmatrix} + \begin{pmatrix} 0 & -i\Sigma_+ & 0 & 0 \\ i\Sigma_+ & 0 & -i\lambda_{XR} & 0 \\ 0 & i\lambda_{XR} & 0 & -i\Sigma_- \\ 0 & 0 & i\Sigma_- & 0 \end{pmatrix}, \quad (\text{B4})$$

where $\mathbf{p} = (p_x, p_y)$ is the momentum operator, with $p_\pm = p_x \pm ip_y$, and v_F^* and v_d^* are renormalized Fermi velocities (see text for their explicit dependence in terms of the Slater-Koster parameters). The diagonal parameters ε_\pm are shift energies defined in Eq.(6). The nondiagonal parameters $\Sigma_\pm = \Delta_- \pm \Delta_+$, with Δ_\pm defined in Eq.(5). Finally the effective spin-orbit parameter λ_{XR} is described in Eq.(3). All these parameters are characterized in a nontrivial way on the overlapping p_z - d integrals and on the exchange field. The effective Hamiltonian (B4) can be written in compact form as given by Eq.(1).

* mperalta@yachaytech.edu.ec

† fmiroles@cnyn.unam.mx

- 1 K. S. Novoselov, V. I. Falko, L. Colombo, P. R. Gellert, M. G. Schwab, K. Kim, Nature **490**, 192 (2012).
- 2 E. Voloshina and Y. Dedkov, Phys. Chem. Phys. **14**, 13502 (2012).
- 3 P. A. Khomyakov, G. Giovannetti, P. C. Rusu, G. Brocks, J. van den Brink, and P. J. Kelly, Phys. Rev. B **79**, 195425 (2009).
- 4 T. Abtew, B.-C. Shih, S. Banerjee, and P. Zhang, Nanoscale **5**, 1902 (2013).
- 5 G. Giovannetti, P. A. Khomyakov, G. Brocks, V. M. Karpan, J. van den Brink, and P. J. Kelly, Phys. Rev. Lett. **101**, 026803 (2008).
- 6 J. Wintterling and M. L. Bocquet, Surf. Sci. Rep. **67**, 83 (2012).
- 7 I. I. Klimovskikh, S. S. Tsirkin, et al. Phys. Rev. B **90**, 235431 (2014).
- 8 Z. Wang, C. Tang, R. Sachs, Y. Barlas, and J. Shi, Phys. Rev. Lett. **114**, 016603 (2015).
- 9 K.-H. Jin and S.-H. Jhi, Phys. Rev. B **87**, 075442 (2013).
- 10 D. Marchenko, A. Varykhalov, M. R. Scholz, G. Bihlmayer, E. I. Rashba, A. Rybkin, A. M. Shikin, and O. Rader, Nat. Comm. **3**, 1232 (2012).
- 11 Varykhalov, A. et al. Phys. Rev. Lett. **108**, 066804 (2012).
- 12 E. I. Rashba, Phys. Rev. B **79**, 161409(R) (2009).
- 13 M. Krivenkov, E. Golias, D. Marchenko, J. Sánchez-Barriga, G. Bihlmayer, O. Rader and A. Varykhalov, 2D Matter. **4**, 035010 (2017).
- 14 M. M. Otrokov, I. I. Klimovskikh, F. Calleja, A. M. Shikin, O. Vilkov, A. G. Rybkin, D. Estyunin, S. Muff, J. H. Dil, A. L. Vázquez de Parga, R. Miranda, H. Ochoa, F. Guinea, J. I. Cerdá, E. V. Chulkov and A. Arnau, 2D Matter. B **5**, 035029 (2018).
- 15 T. P. Cysne, A. Ferreira, and T. G. Rappoport, Phys. Rev. B **98**, 045407 (2018).
- 16 A. López, L. Colmenárez, M. Peralta, F. Mireles, and E. Medina, Phys. Rev. B **99**, 085411 (2019).
- 17 S. Kunschuh, M. Gmitra, and J. Fabian, Phys. Rev. B **82**, 245412 (2010).
- 18 H. Min, J. E. Hill, N. A. Sinitsyn, B. R. Sahu, L. Kleinman and A. H. MacDonald, Phys. Rev. B **74**, 165310 (2006).
- 19 E.V. Zhizhin, A. Varykhalov, et al. Carbon **93**, 984 (2015).
- 20 H. X. Yang, A. Hallal, D. Terrade, X. Waintal, S. Roche, and M. Chshiev, Phys. Rev. Lett. **110**, 046603 (2013).
- 21 H. Chen, Q. Niu, Z. Zhang, and A. H. MacDonald, Phys. Rev. B **87**, 144410 (2013).
- 22 M. Peralta, L. Colmenarez, A. López, B. Berche and E. Medina, Phys. Rev. B **94**, 235407 (2016).
- 23 P. T. Vo, N. R. Walet, and F. P. Guinea, 2D Mater. **5**, 014004 (2017).
- 24 V. T. Phong, N. R. Walet and F. Guinea, 2D Mater. **5**, 014004 (2018).
- 25 D. Usachov, A. Fedorov, M. M. Otrokov, A. Chikina, O. Vilkov, A. Petukhov, A. G. Rybkin, Y. M. Koroteev, E. V. Chulkov, V. K. Adamchuk, A. Gruneis, C. Laubschat,

- and D. V. Vyalikh, *Nano Lett.* **15**, 2396 (2015).
- ²⁶ A. G. Rybkin, A. A. Rybkina, M. M. Otrokov, O. Vilkov, I. I. Klimovskikh, A. E. Petukhov, M. V. Filianina, V. Y. Voroshnin, I. P. Rusinov, A. Ernst, A. Arnau, E. V. Chulkov and A. M. Shikin, *Nano Lett.* **18**, 1564-1574 (2018).
- ²⁷ A. Varykhalov, D. Marchenko, J. Sánchez-Barriga, M. R. Scholz, B. Verberck, B. Trauzettel, T. O. Wehling, C. Carbone, and O. Rader, *Phys. Rev. X* **2**, 041017 (2012).
- ²⁸ D. Marchenko, A. Varykhalov, J. Sánchez-Barriga, O. Rader, C. Carbone, and G. Bihlmayer, *Phys. Rev. B* **91**, 235431 (2015).
- ²⁹ Hereafter we shall use the short notation z^2 for the orbitals $3z^2 - r^2$ of the ferromagnetic metals.
- ³⁰ Data inferred from the SARPES bands reported in Ref.[27] for the case of graphene/Ni and from Ref.[28] for graphene/Co.
- ³¹ A. Saffarzadeh and G. Kirczenow, *Phys. Rev. B* **85**, 245429 (2012)
- ³² E.C. Stoner, *Proc. R. Soc. A, Math. Phys. Eng. Sci.* **165**, 372 (1938).
- ³³ C. Barreteau, D. Spanjaard, and M.C. Desjonqueres, *C. R. Physique* **17**, 406-429 (2016).
- ³⁴ S. Roche, J. Åkerman, B. Beschoten, J.-C. Charlier, M. Chshiev, S.P. Dash, B. Dlubak, J. Fabian, A. Fert, M. Guimaraes, F. Guinea, I. Grigorieva, C. Schonenberger, P. Seneor, C. Stampfer, S. O. Valenzuela, X. Waintal and B. van Wees, *2D Mater.* **2**, 030202 (2015).
- ³⁵ J. C. Slater, and G. F. Koster, *Phys. Rev.* **94**, 1498 (1954).
- ³⁶ E. McCann, and M. Koshino, *Rep. Prog. Phys.* **76**, 056503 (2013).